FOURTEENTH EUROPEAN ROTORCRAFT FORUM

Paper No. 59

ACTIVE CONTROL OF TILT-ROTOR BLADE IN-PLANE LOADS DURING MANEUVERS

DAVID G. MILLER
BOEING HELICOPTER CO.
PHILADELPHIA, PA., U.S.A.

NORMAN D. HAM
MASSACHUSETTS INSTITUTE OF TECHNOLOGY
CAMBRIDGE, MASSACHUSETTS, U.S.A.

20-23 September, 1988
MILANO, ITALY

ASSOCIAZIONE INDUSTRIE AEROSPAZIALI
ASSOCIAZIONE ITALIANA DI AERONAUTICA ED ASTRONAUTICA

ACTIVE CONTROL OF TILTROTOR BLADE IN-PLANE LOADS DURING MANEUVERS

David G. Miller
Boeing Helicopter Company
Philadelphia, PA 19142 USA

Norman D. Ham
Massachusetts Institute of Technology
Cambridge, MA 02139 USA

Abstract

The origin of one/rev rotor aerodynamic loads which arise in tiltrotor aircraft during airplane-mode high speed pull-up and push-over maneuvers is examined using a coupled rotor/fuselage dynamic simulation. A modified eigenstructure assignment technique is used to design a controller which alleviates the in-plane loads during high pitch rate maneuvers. The controller utilizes rotor cyclic pitch inputs to restructure the aircraft short period and phugoid responses in order to achieve the coupling between pitch rate and rotor flapping responses which minimizes the rotor aerodynamic loading. Realistic time delays in the feedback path are considered during the controller design. Stability robustness in the presence of high frequency modelling errors is ensured through the use of singular value analysis.

1. Introduction

1.1 Motivation for Research

The tiltrotor aircraft offers the advantages of low speed operability and vertical take-off or landing capability of a helicopter, while providing the efficiency and comfort of high speed airplane mode flight. The tiltrotor aircraft can potentially fulfill a wide variety of commercial, military, and law enforcement missions. Presently, however, most proposed tiltrotor applications have been in the air transport category. The agility offered by the tiltrotor design has not been fully exploited, in part because of concern about high rotor loads encountered during aggressive maneuvers.

This paper will focus on the development of in-plane rotor loads in the tiltrotor during high speed, airplane-mode, pitch axis maneuvers. The level of in-plane bending moments exerted on the rotor blades has been shown [1] to be the limiting factor of g capability of the tiltrotor aircraft. The stiff in-plane rotor configuration which is proposed for most tiltrotor designs allows no inertial relief of the blade in-plane moments through lagging motion of the rotor blade about a lag hinge. As a result, in-plane moments exerted on the rotor blade result directly in yoke chord bending moments. If the yoke chord bending moments exceed the structural limit load of the blade, severe damage to the rotor system may occur.

The objective of this research is twofold. First the origin of the in-plane loads in high speed flight will be investigated. Second, an understanding of the physics of the phenomenon will be used to propose a means of alleviating the in-plane loads problem. It is shown that a firm physical explanation of the dynamics of the in-plane loads, together with the sophisticated computer-aided control system design software available today, can produce a feasible solution to the problem.

This research was sponsored by the Ames Research Center (NASA-MIT Cooperative Agreement NCC-2-366) and the Boeing Helicopter Company.

1.2 Previous Research

The maneuverability and agility characterisitcs of the tiltrotor aircraft are discussed in a paper by Schillings et. al. [1], wherein the authors show that blade one/rev in-plane loads in high speed flight are directly related to aircraft pitch rate. An advanced pitch axis controller is developed in [1] which effectively limits the maximum transient pitch rate attainable by the aircraft in response to pilot commands. The solution presented in [1] essentially uses feedback of aircraft pitch rate to the elevator to produce a closed-loop pitch rate response to disturbances and pilot inputs which is smaller, both in transient and steady state conditions, than the open-loop response. Although the ref. [1] controller limits the relative magnitude of aircraft pitch rate, the amount of in-plane moment for a given magnitude of pitch rate is basically unaltered by pitch rate feedback to the elevator.

The study conducted in [1] uses several mathematical models to predict the aircraft behavior. A nonlinear coupled rotor/fuselage analysis (C81) [2] is compared to the generic tiltrotor simulation (GTRS) program [3], an analysis which is used primarily for real-time piloted simulation. Comparison of both analyses with flight test [1] shows a high degree of fidelity in predicting the in-plane loads during pitch axis maneuvers. The GTRS model uses nonlinear fuselage equations of motion coupled with linear rotor flapping equations, in which only the lower frequency rotor flapping dynamics are approximated by coupled first order lags, to represent the in-plane loads phenomenon. The high degree of fidelity achieved by the linearized rotor model in representing flight test behavior indicates that a linear rotor model can adequately represent the pertinent dynamics of the in-plane loads phenomenon. It has also been shown [4] that linearized rigid body aircraft models can accurately model aircraft behavior for single axis pitch rate maneuvers up to very high pitch rates and and high angles of attack. As a result, a linear, coupled rotor/fuselage analysis can be used to simulate the in-plane loads dynamics.

During helicopter-mode flight, the aircraft relies on swashplate inputs to provide the forces and moments necessary to control the aircraft. During transitional flight from helicopter-mode to airplane-mode flight a combination of swashplate and airframe control surface inputs, including flap, aileron, rudder, and elevator deflections, are used to control the aircraft. In high speed airplane-mode flight, the tiltrotor relies entirely on airframe control surface deflections to provide acceptable handling qualities. Recent studies [5,6] indicate that active control of helicopter blade motion through swashplate inputs can provide gust alleviation, vibration suppression, and flapping stabilization in helicopters. Thus active control of the rotor blades through swashplate inputs in airplane-mode flight will be considered as a means to alleviate the in-plane loads.

This paper will concern itself with the control of a three bladed rotor system, wherein the method of multiblade coordinates [7] can be used to eliminate the periodicity from the coupled rotor/fuselage equations of motion. The resulting linear constant coefficient system will include the cyclic and collective pitch angles of the rotor blades as the control input terms. It is shown by Ham [8] that there is an equivalence between active one/rev control using a conventional swashplate arrangement, relying on lateral and longitudinal cyclic pitch and collective pitch, and individual blade actuation for a three bladed rotor system. As a result, the methodologies developed for control and estimation of the rotor blade motion within the scope of individual-blade-control (IBC) research may be applied to the problem. Therefore one can use appropriately filtered blade mounted sensor information [9] to provide an accurate estimate of rotor blade motion.

Several powerful design methodologies exist for the control of multivariable linear systems. Generally, these design techniques can be categorized as either time domain or frequency domain approaches. Frequency domain methods use graphical techniques to characterize system performance as a function of input command or disturbance frequency, while time domain techniques characterize performance in terms of the time responses of the variables of interest in the system [10-14].

The time domain design approach considered here is eigenstructure assignment [15], wherein constant gain output feedback is used to assign the system closed-loop poles and right eigenvectors. A great deal of insight into the sytem dynamics is required to make an appropriate choice of the desired eigenvalues and eigenvectors. A poor choice of the desired eigenstructure may result in a system which exhibits unacceptable performance, execessive control usage, or poor robustness characteristics. For systems in which the phenomenon of interest is associated with a particular dynamic mode, and there exists sufficient knowledge to make an appropriate choice of eigenstructure, the eigenstructure assignment approach can be used to address both time and frequency domain criteria. Also, the design need not be optimized for a specific type of input because the form of the right eigenvectors will shape the system response for any set of initial conditions or control inputs.

As mentioned previously, the in-plane loads have been shown to be directly related to the aircraft pitch rate. The rapid rotation of the airplane in pitch is predominantly due to the dynamics of the short period mode [16]. As a result, appropriate phasing of the rotor and airframe responses during the short period response presents a possible means of alleviating the in-plane rotor loads.

The aircraft angle of attack and pitch rate responses are dictated by handling qualities criteria. Thus knowledge of the desired short period pole location, and desired phasing of the aircraft angle of attack and pitch rate responses will be taken as a given for this analysis. A controller which modifies the eigenstructure in the low frequency range, while leaving higher frequency modes unchanged, should be robust to high frequency modelling errors. Thus by designing a controller which modifies only the short period dynamics, which occur in the vicinity of one cycle per second, robustness to modelling errors of the higher frequency rotor dynamics, which occur above four cycles per second, can be ensured.

1.3 Scope of Research

An overview of the coupled rotor/fuselage model used to represent the tiltrotor aircraft is presented in chapter 2. The simulation model includes six degree of freedom rigid body motion and rotor flapping dynamics. Cyclic pitch actuator dynamics are modelled as a 0.1 second time delay using Pade approximations. The combination of rigid body, rotor, and actuator dynamics results in a state space description of the aircraft which contains 29 states.

An explanation of the relationship between in-plane loads and aircraft pitch rate in the tiltrotor in high speed, airplane-mode flight is offered in chapter 3. Basic aerodynamic and mechanical principles are exploited to yield a tractable expression for the in-plane loads in terms of the system state variables. The one/rev in-plane loads are shown to be a function of rotor cyclic flapping and blade pitch angles, and aircraft pitch rate and angle of attack.

Chapters 4 and 5 describe the controller design process. Chapter 4 reviews eigenstructure assignment methodology using constrained state feedback. A controller is then developed which minimizes in-plane moments by properly phasing aircraft rigid body motion, rotor cyclic flapping, and cyclic pitch inputs. Chapter 5 then considers adapting the controller design to operate within realistic cyclic pitch authority limits.

2. Mathematical Model Description

2.1 Introduction

A mathematical model of the aircraft should be sufficiently sophisticated to represent the pertinent dynamics of the in-plane loads. The math model should not, however, be so detailed as to hopelessly complicate the control system design process. Powerful control system design techniques exist for linear time invariant (LTI) systems, therefore a linearized model is developed which represents the in-plane loads in the frequency range of interest. A description of the generic modelling algorithm used to represent the tiltrotor aeromechanical characteristics is given in the following sections.

2.2 Exponential Basis Function Technique

The task of formulating a representative rotor/fuselage mathematical model has always been complicated by the large number of coordinate transformations necessary to define the rotor position and orientation in inertial space. The algebra involved in the derivation of the simplest rotor model is formidable, making manual derivation of the equations tedious and prone to error. In order to minimize the human effort involved in the derivation process, thereby reducing the risk of modelling errors, it is necessary to utilize a computer-aided modelling algorithm.

The approach taken in this analysis differs substantially from the computational methods of [17] and [18]. The task of deriving the equations of motion which involve many coordinate transformations can be simplified if the position vectors, describing the location of all the mass elements in the system, can be written in a form which can be easily manipulated. The underlying idea is to express the coordinate transformations required in the math model in a structure which is easily retained throughout each phase of the derivation process.

One of the operations which complicates the derivation of the equations of motion is axis transformation from one coordinate system to another. Coordinate transformations are most easily accomplished by means of multiplication of transformation matrices, where each transformation matrix represents a rotation about a particular coordinate axis. It can be shown [19] that the elements of all transformation matrices can be written as a summation of exponential functions whose arguments consist only of the coordinate transformation angles. Multiplication of the coordinate transformation matrices results in addition of the arguments of the exponential functions. A second operation which yields great algebraic complexity is the time differentiation of the position vector to obtain the velocity and acceleration terms in the equations of motion. Linearization can also be accomplished by partial differentiation of the nonlinear equations of motion with respect to the state variables to obtain the coefficients of the state variables in the dynamic equations. As a result, formulation of the position vector in terms of exponential basis functions, perhaps the simplest functions to differentiate, also simplifies the derivation process. The reader is referred to [19] for a complete treatment of the exponential basis function (EBF) simulation generation process.

2.3 Tilt Rotor Modelling Points

A single rotor helicopter simulation based on the exponential basis function algorithm has been favorably correlated with flight test data (19). In light of the correlation of the exponential basis function simulation and flight test data, it is reasonable to assume that the coupled rotor/fuselage equations derived for the tiltrotor aircraft using the EBF algorithm have a high degree of fidelity. Although there are many similarities in the general structure of the tiltrotor and single rotor helicopter defining equations, there are several differences in the two types of vehicles which necessitate modification of the math model generation software. The most significant of these software modifications are described below.

The gimballed rotor configuration of the tiltrotor is represented in the math model by a modified, low hinge offset, articulated rotor system. The gimbal is represented by modifying the multiblade coordinate flapping equations by adding a relatively small cyclic flapping spring term to the cyclic flapping equations, and a large coning spring term to the coning equations. The cyclic flapping spring represents the effect of the gimbal hub spring, while the coning spring represents the effect of blade flexibility. The simulation can thus allow for motion of the tip path plane about the gimbal axes, as well as represent in-phase coning motion of the blades out of the gimbal plane. The advantage in this approach is to represent both the low frequency flapping due to gimbal motion and the higher frequency first harmonic flapping due to blade flexibility by using only three dynamic degrees of freedom. An exact representation of the gimballed rotor system requires two degrees of freedom to represent gimbal motion, and three more dynamic degrees of freedom to represent the out-of-plane bending of each of the three rotor blades.

Current tiltrotor designs utilize a constant speed joint to eliminate two/rev drive system loads [20]. The constant speed joint maintains constant rotational velocity in the gimbal axis system, effectively aligning the rotor angular velocity vector in a direction normal to the gimbal plane. As a result, the rotor precesses in a manner similar to a rigid cone when undergoing cyclic flapping motion, engendering no blade one/rev chordwise coriolis moments. The action of the constant speed joint is taken into account by a separate derivation of the in-plane moment equations using Euler's equations of motion.

Displacement of the pitch housing relative to the swashplate is a result of the combined effect of gimbal tilt and blade flexibility. As a result, the blade pitch/flap coupling is itself a function of azimuth. In order to represent this phenomenon, the equations of motion were modified to account for different amounts of blade pitch change due to cyclic flapping motion and coning motion.

The equations of motion of the single rotor helicopter simulation [19] had been represented in an inertial axis system. In keeping with standard airplane control system design practice, a transformation of coordinates to a stability [16] axis system was undertaken. The resulting equations of motion were then modified to account for downwash perturbations on the horizontal tail induced by changes in wing lift.

The resulting linearized rotor/fuselage model contains twelve dynamic degrees of freedom. In addition to the six degrees of freedom of rigid body motion, there is a degree of freedom associated with the flapping motion of each of the three rotor blades on each of the aircraft's two rotors. The aircraft rigid body states included in the simulation are body axis pitch, roll, and yaw angular rates; Euler pitch, roll, and yaw angles; and integral and proportional body axis vertical, longitudinal, and lateral velocity states. Coleman coordinates are used to express the rotor equations in constant coefficient form, using lateral cyclic, longitudinal cyclic, and coning blade flapping angles and rates. Actuator dynamics are represented as pure time delays through Pade approximations. The Pade approximations introduce additional first order differential equations, wherein the elevator and rotor cyclic pitch angles are included as dynamic states, which increase the number of state variables in the simulation to twenty-nine. Table 2.1 details the dynamic modes associated with the nominal 260 knot, aft center of gravity condition considered in this analysis. The numbering system used to reference each state in the model, and the physical units of each of the state variables, is given in Table 2.2.

3. Physics of In-Plane Loads In Tiltrotors At High Speeds

3.1 Introduction

Euler's equations of motion can be used to formulate the equations of motion of the gimballed rotor system. Fundamental mechanics and linear aerodynamics can then be used to derive the in-plane moments exerted on the rotor blades. The resulting equations contain a compact representation of the effect of rigid body aircraft motion, cyclic flapping, and rotor cyclic pitch inputs on in-plane rotor loads. The form of the in-plane moment equations allows for a physically satisfying explanation of some of the counter-intuitive aspects of tiltrotor behavior in high speed flight.

3.2 Derivation of Out-of-Plane Precessional Moment Equations

In order to precess the rotor at the aircraft pitch rate a net gyroscopic moment must be exerted on the rotor system. The precessional moment will be made up mainly of one/rev aerodynamic moments exerted on the rotor blades and partially by hub moments exerted by the gimbal spring restraint. Referring to Figure 3.1, Euler's equations of motion for the external moments exerted on the system can be written:

$$\underline{M} = \frac{\partial \underline{A}}{\partial t} + \underline{\omega} \times \underline{A} \qquad (3.1)$$

where $\underline{A}$ is the angular momentum vector expressed in the gimbal axis system, and $\underline{\omega}$ is the angular velocity of the gimbal axis coordinate system with respect to a fixed frame. The angular momentum in the gimbal frame is given by:

$$\underline{A} = -3I_\beta \Omega \, \underline{k} \tag{3.2}$$

Noting the assumed equivalence between cyclic flapping and gimbal motion, one can use the cyclic flapping expression

$$\beta = a_1 \cos \Psi_n + b_1 \sin \Psi_n \tag{3.3}$$

to obtain the angular velocity of the gimbal frame with respect to a fixed frame of reference.

$$\underline{\omega} = \dot{b}_1 \, \underline{i} - (q - \dot{a}_1) \underline{j} \tag{3.4}$$

The constant speed joint ensures that when shaft RPM is constant the angular momentum in the gimbal axis system is conserved. Therefore, one can write:

$$\partial \underline{A} / \partial t = 0 \tag{3.5}$$

Performing the cross-product operation in eqn. (3.1) yields the external moments exerted on the rotor system:

$$\underline{M} = 3I_\beta \Omega (q - \dot{a}_1) \underline{i} + 3I_\beta \Omega (\dot{b}_1) \underline{j} \tag{3.6}$$

The external moments exerted on the rotor system will be composed of a combination of aerodynamic and hub moments. The moments exerted on the hub which result from the nth blade reacting against the gimbal spring restraint, resolved about the x and y gimbal axes, are given by:

$$\begin{aligned} M_x &= -K_\beta \beta \sin \Psi_n \\ M_y &= -K_\beta \beta \cos \Psi_n \end{aligned} \tag{3.7}$$

where K_β is the gimbal spring constant and β is the cyclic flapping angle. The total hub moments exerted by the gimbal spring are the result of the actions of each of the three rotor blades,

$$M_x = \sum_{n=1}^{3} - K_\beta (a_1 \cos \Psi_n + b_1 \sin \Psi_n) \sin \Psi_n \tag{3.8}$$

$$M_y = \sum_{n=1}^{3} - K_\beta (a_1 \cos \Psi_n + b_1 \sin \Psi_n) \cos \Psi_n \tag{3.9}$$

therefore:

$$\begin{aligned} M_x &= -\frac{3}{2} K_\beta b_1 \\ M_y &= -\frac{3}{2} K_\beta a_1 \end{aligned} \tag{3.10}$$

The harmonic portion of the aerodynamic out-of-plane moments exerted on each rotor blade can now be expressed as:

$$M_T = M_{T_C} \cos \Psi_n + M_{T_S} \sin \Psi_n \tag{3.11}$$

The net gimbal axis moments exerted on the rotor system will be given by:

$$\begin{aligned} M_x &= \sum_{n=1}^{3} M_T \sin \Psi_n = \frac{3}{2} M_{T_S} \\ M_y &= \sum_{n=1}^{3} M_T \cos \Psi_n = \frac{3}{2} M_{T_C} \end{aligned} \tag{3.12}$$

Adding the gimbal spring and out-of-plane aerodynamic moments yields the sum of out-of-plane moments equation:

$$\begin{aligned} -\frac{3}{2} K_\beta b_1 + \frac{3}{2} M_{T_S} &= 3I_\beta \Omega (q - \dot{a}_1) \\ -\frac{3}{2} K_\beta a_1 + \frac{3}{2} M_{T_C} &= 3I_\beta \Omega \dot{b}_1 \end{aligned} \tag{3.13}$$

Solving for the one/rev out-of-plane aerodynamic moments exerted on each blade gives:

$$\begin{aligned} M_{T_S} &= 2I_\beta \Omega (q - \dot{a}_1) + K_\beta b_1 \\ M_{T_C} &= 2I_\beta \Omega (\dot{b}_1) + K_\beta a_1 \end{aligned} \tag{3.14}$$

3.3 Derivation of In-Plane Moment Equations

Now consider how the out-of-plane aerodynamic moments required to precess the rotor relate to the in-plane blade moments. Figure 3.2 shows the relative wind and airfoil geometry for the high inflow condition. One can neglect the aerodynamic drag forces on the rotor blade element to write the in-plane and out-of-plane aerodynamic forces exerted on the rotor as:

$$\begin{aligned} dH &= dL \sin \phi \\ dT &= dL \cos \phi \end{aligned} \tag{3.15}$$

where one can use the exact expression for thin airfoil lift due to angle of attack to obtain the lift force:

$$dL = \frac{1}{2} \rho \, a \, c \, U^2 \sin (\alpha) \, dr \tag{3.16}$$

For convenience, collect the air density, lift curve slope, differential radial element length, and blade chord length constants into one constant given by:

$$C_A = \frac{1}{2} \rho \, a \, c \, dr \tag{3.17}$$

First, in order to gain a general understanding of the relationship between H-force and thrust force in the tilt-rotor at high speed, consider only the aerodynamic forces at the three-quarter radius location. For the high inflow condition, the inflow angle ϕ will be on the order of 45 degrees. Thus small angle approximations for the inflow angle are not valid. In airplane-mode flight the rotor operates as a propeller, generating only enough thrust to overcome the relatively small aerodynamic drag forces exerted on the aircraft. As a result, the lift produced by the rotor will be much smaller than the helicopter mode lift which is required to sustain the gross weight of the aircraft. Therefore, the angle of attack of the blade element, given by the difference of the blade geometric pitch angle θ and the inflow angle, will be small and one can safely use small angle approximations for the θ-ϕ term to obtain:

$$\begin{aligned} dH &= C_A U^2 (\theta - \phi) \sin \phi \\ dT &= C_A U^2 (\theta - \phi) \cos \phi \end{aligned} \tag{3.18}$$

Taking the variation of the in-plane and thrust forces gives:

$$\delta(dH) = [2C_A U(\theta - \phi) \sin \phi]\, \delta U + [C_A U^2 \sin \phi)\, (\delta\theta - \delta\phi) + [C_A U^2 (\theta - \phi) \cos \phi]\, \delta\phi \tag{3.19}$$

$$d(dT) = [2C_A U(\theta - \phi) \cos \phi]\, \delta U + [C_A U^2 \cos \phi]\, (\delta\theta - \delta\phi) + [-C_A U^2 (\theta - \phi) \sin \phi]\, \delta\phi$$

An order of magnitude analysis can be used to simplify the expressions above to include only the dominant terms:

$$d(dH) \approx [C_A U^2 \sin \phi]\, (\delta\theta - \delta\phi)$$
$$d(dT) \approx [C_A U^2 \cos \phi]\, (\delta\theta - \delta\phi) \tag{3.20}$$

Inspection of the equations above reveals that the incremental thrust and H-force perturbations from trim are proportional and related by:

$$\delta(dH)/\delta(dT) = \tan \phi \tag{3.21}$$

The thrust and H-forces act through the same radial moment arm, therefore the incremental in-plane and out-of-plane aerodynamic moments contributed by the blade element are also proportional. The simplified expression above predicts that the ratio of the in-plane to out-of-plane aerodynamic moments increases as the airspeed, hence inflow angle, increases. The insight gained from the simplified three-quarter radius analysis is that a greater percentage of the required out-of-plane moment is exerted as a chordwise bending moment on each of the rotor blades as airspeed increases.

In order to obtain a more precise relationship between the in-plane and out-of-plane aerodynamic moments, a spanwise integration analysis is presented which accounts for the variation in rotor aerodynamic properties with radial location. Referring again to Figure 3.2, one can note:

$$\sin \phi = U_P/U$$
$$\cos \phi = U_T/U \tag{3.22}$$

One can therefore write the incremental thrust and H-forces by substituting eqns. (3.22) into eqns. (3.15) and (3.16):

$$dH = C_A U^2 \sin (\theta - \phi)\, U_P/U$$
$$dT = C_A U^2 \sin (\theta - \phi)\, U_T/U \tag{3.23}$$

Using the trigonometric identities for the sine and cosine of the sum of two angles yields:

$$dH = C_A U U_P [\sin \theta \cos \phi - \cos \theta \sin \phi]$$
$$dT = C_A U U_T [\sin \theta \cos \phi - \cos \theta \sin \phi] \tag{3.24}$$

Using the expressions for $\sin(\varphi)$ and $\cos(\varphi)$ from eqns. (3.22) gives:

$$dH = C_A [\sin \theta\, U_P U_T - \cos \theta\, U_P^2]$$
$$dT = C_A [\sin \theta\, U_T^2 - \cos \theta\, U_P U_T] \tag{3.25}$$

The perturbation in-plane and out-of-plane aerodynamic forces can be obtained by taking the variation of the above:

$$\delta(dH) = C_A \{[\sin \theta\, U_P]\, \delta U_T + [\sin \theta\, U_T - 2 \cos \theta\, U_P]\, \delta U_P + [\cos \theta\, U_P U_T + \sin \theta\, U_P^2]\, \delta\theta\} \tag{3.26}$$

$$\delta(dT) = C_A \{[2 \sin \theta\, U_T - \cos \theta\, U_P]\, \delta U_T + [-\cos \theta\, U_T]\, \delta U_P + [\cos \theta\, U_T^2 + \sin \theta\, U_P U_T]\, \delta\theta\}$$

One can use the approximate expressions for perturbation tangential and perpendicular relative wind velocities and geometric blade angle given below:

$$\delta U_P = r(\dot\beta - q \cos \Phi)$$
$$\delta U_T = \delta W \sin \Phi \tag{3.27}$$
$$\delta\theta = \theta_{1c} \cos \Phi + \theta_{1s} \sin \Phi$$

to rewrite the perturbation integral thrust and H-force moment expressions, given below, in terms of the system state variables.

$$\delta M_H = {}_0\int^R \delta(dH)\, r \tag{3.28}$$
$$\delta M_T = {}_0\int^R \delta(dT)\, r$$

Substituting the actual flight conditions and rotor geometry given in Appendix A into the expressions above, and then integrating the product of the radial moment arm and the incremental thrust and H-forces, yields the perturbation in-plane and out-of-plane aerodynamic moments.

$$\delta M_H = (12032.46)(\dot\beta - q \cos \Phi) + (901347.94)\, \delta\theta + (1030.53)(\delta W \sin \Phi) \tag{3.29}$$

$$\delta M_T = (14985.18)\, (\dot\beta - q \cos \Phi) + (956760.61)\, \delta\theta + (1022.39)\, (\delta W \sin \Phi)$$

The expressions above indicate that the thrust and in-plane moment perturbations are very similar in form. In order to assess the differences in the expressions, subtract a multiple of the perturbation thrust moment from the perturbation in-plane moment to obtain:

$$\delta M_H - 0.8\delta M_T = (133110)\, \delta\theta + (209.59)\, \delta W \sin \Phi \tag{3.30}$$

Remembering the expression derived for the aerodynamic out-of-plane moment in eqn.(3.14), one can express the in-plane moment as:

$$\delta M_H = 0.8\{[2(q - \dot a_1)\, I_\beta \Omega + K_\beta b_1] \sin \Phi + (133110)\, \delta\theta + 209.59\, (\delta W \sin \Phi) + [2\dot b_1 I_\beta \Omega + K_\beta a_1] \cos \Phi\} \tag{3.31}$$

Finally, the one/rev in-plane moments exerted on the rotor blade are given by:

$$\delta M_H = \{0.8[2I_\beta\Omega(q-\dot{a}_1) + K_\beta b_1] + 133110\ \theta_{1s} + 209.59\ \delta W\}\ \sin\Psi + \{0.8[2I_\beta\Omega\ \dot{b}_1 + K_\beta a_1] + 133110\ \theta_{1c}\}\ \cos\Psi \tag{3.32}$$

3.4 Intuitive Concepts

Presented in Figure 3.3 is a time history of an open-loop aft longitudinal stick step at 260 knots. An order of magnitude analysis reveals that the most significant contribution to the in-plane moment is made by the term $(q - \dot{a}_1)$. As the aircraft pitches nose-up, the tip-path-plane actually leads the shaft angular velocity. This unusual behavior can be attributed to the unique operating conditions of the tiltrotor.

First consider the approximate relationships for incremental thrust and H-force of eqn. (3.20). The change in thrust and H-force is very nearly proportional to the change in angle of attack. For the case of fixed rotor blade pitch, the rotor will experience a change in angle of attack given by:

$$\delta\alpha = -\delta\theta = -\delta[\tan^{-1}(U_P/U_P)]$$

$$\delta\alpha = \frac{U_T}{U_P^2+U_T^2}\ \{\delta U_T U_P/U_T - \delta U_P\} \tag{3.33}$$

In a typical low inflow condition, the ratio of the trim out-of-plane velocity to the trim in-plane-velocity is small, thus angle of attack changes are due primarily to changes in *the out-of-plane velocity.* In the high inflow condition, however, the ratio of the tangential and perpendicular velocities is close to unity. As a result, changes in the tangential velocity can significantly change the blade section angle of attack.

Now consider the change in angle of attack at ψ=90 degrees which gives rise to the longitudinal flapping response of the rotor. The change in tangential velocity for the high speed pull-up maneuver is due largely to the body axis vertical velocity and given approximately by eqn. (3.27). At high speed, the change in the vertical body axis velocity is large. The change in the out-of-plane velocity is due primarily to longitudinal flapping and can be written:

$$\delta U_P = -a_1\ \Omega\ r\ \sin\Psi \tag{3.34}$$

The change in angle of attack is given by:

$$\delta\alpha = \frac{U_T}{(U_P^2+U_T^2)}\quad \delta W\frac{U_P}{U_T} + a_1\ \Omega\ r \quad \sin\Psi \tag{3.35}$$

Particularizing the expression above for the conditions at the three-quarter radius location and assuming that the ratio of the in-plane and out-of-plane velocities is unity gives:

$$\delta\alpha = \frac{1}{2\ \Omega\ R\ (0.75)}\ [\delta W + a_1\ \Omega(0.75)R]\ \sin\Psi \tag{3.36}$$

The aerodynamic portion of the precessional moment for a nose-up pitch rate must be supplied by a positive angle of attack change at ψ=90 degrees. The angle of attack change induced by the δW velocity alone is greater than the angle of attack change needed to produce the precessional moment. As a result, a negative longitudinal flapping angle, corresponding to the tip path plane leading the shaft normal plane as the shaft pitches nose-up, is necessary to maintain moment equilibrium during the pull-up maneuver. As the body axis velocity δW builds up during the maneuver, the longitudinal flapping angle becomes increasingly negative, hence a negative longitudinal flapping rate is produced.

The most significant term in the in-plane moment expression was shown to be given by:

$$\delta M_H \approx 2\ I_\beta\Omega\ (q - \dot{a}_1)\ \sin\Psi \tag{3.37}$$

The large body-axis vertical velocity induced by the pull-up maneuver at high speed and the high inflow condition of the rotor result in the curious effect of the pitch rate and tip path plane precessional rate occurring in the same direction. As a result the magnitude of the pitch rate and longitudinal flapping angular rate sum to give a large one/rev in-plane bending moment.

The one/rev in-plane moments have been shown to be a consequence of airplane pitch rate. Thus reducing the aircraft pitch rate whenever possible is one approach to alleviating the in-plane loads. Figure 3.5 illustrates the effect of pitch rate feedback to elevator angle, similar to the ref. [1] controller design, on the longitudinal stick step responses. The presence of this type of feedback results in smaller pitch rates, hence lower in-plane moments, than the open-loop responses.

Rotor cyclic pitch inputs can be used to modify the angle of attack, and hence aerodynamic forces and moments, experienced by the rotor blades. Through modification of the one/rev aerodynamic forces and moments exerted on the blade, the optimum rotor flapping responses for in-plane loads reduction can be produced. Shown in Figure 3.6 is a block diagram of the combined rotor cyclic pitch and elevator controller which is to be examined in subsequent chapters. The controller utilizes feedback of the system state variables to the elevator, left rotor longitudinal and lateral cyclic pitch, and right rotor lateral and longitudinal cyclic pitch to alleviate the one/rev blade in-plane loads.

4. Eigenstructure Assignment Methodology

4.1 Introduction

The optimal solution to the tiltrotor *maneuvering loads problem is the design of a* controller which drives the sine and cosine components of the in-plane moment expressions presented in eqn. (3.32) to zero. The in-plane loads arise as a function of the aircraft pitch rate and the ensuing increase in aircraft angle of attack. As a result, a controller which minimizes the aircraft pitch rate will ensure that the in-plane loads remain small. *Unfortunately, it is sometimes necessary for* the pilot to execute high pitch rate maneuvers in order to adequately perform his mission. As a result, the blade in-plane loads controller should be designed to satisfy the more stringent requirement of driving the loads toward zero even when the aircraft sustains a substantial pitch rate.

Constraints introduced by the physics of the rotor/airframe interaction, limits on the allowable blade *flapping responses and cyclic pitch inputs, and time delays in the controller* operation will define the achievable reduction in rotor loads. Additionally, the controller must be designed to operate in the presence of a wide variety of pilot inputs, many of which develop aggressive pitch rates. The problem considered here is to find the controller which minimizes the in-plane loads without adversely affecting the handling qualities of the aircraft.

4.2 Eigenstructure Analysis

The response of a linear time invariant system expressed in the form:

$$\dot{\underline{x}} = A\underline{x} + B\underline{u} \tag{4.1}$$

is given by:

$$\underline{x}(t) = \sum_{i=1}^{n} \underline{v}_i \underline{w}_i \left(\underline{\xi} e^{\lambda_i t} + \int_0^t \sum_{k=1}^{m} \underline{b}_k u_k(\tau) \; e^{\lambda_i (t-\tau)} d\tau \right) \tag{4.2}$$

where λ_i, $\underline{v}_i$, and $\underline{w}_i$ are respectively the eigenvalues, and the right and left eigenvectors of the state matrix A; $\underline{\xi}$ is the initial state ; and u_k are the control inputs. For any combination of initial conditions and control inputs, the state response will be defined by the form of the right eigenvectors of the state matrix A. The relationship between the individual state responses will be determined by the magnitude of the components of each state in the eigenvectors of the system. If one desires a particular relationship between any set of states, the proper shaping of components of the eigenvector will ensure that the given relationship between the states is satisfied for any type of input or initial condition.

In order to minimize the one/rev in-plane moments a specific relationship must exist between the aircraft pitch rate, vertical body axis velocity, rotor cyclic pitch angles, and longitudinal and lateral flapping responses. To eliminate completely the one/rev in-plane aerodynamic moments, both the sine and cosine components of the right-hand side of eqn. (3.32) must equal zero. The two simultaneous equations which must be satisfied to eliminate the one/rev in-plane moments are given below.

$$\begin{aligned} &0.8[2\, I_\beta\, \Omega(\underline{q}-\dot{a}) + K_\beta b_1] + 133110\, \theta_{1s} + 209.59\, \delta W = 0 \\ &0.8[2\, I_\beta\, \Omega\dot{b}_1 + K_\beta a_1] + 133110\, \theta_{1c} = 0 \end{aligned} \tag{4.3}$$

The high speed pull-up maneuver described in Fig. 3.3 is dominated by the short period response of the aircraft. Assuming that only the short period mode is excited during the maneuver, the relationship between the state vector and the time derivative of the state vector is given by:

$$\dot{\underline{x}} = \mu_{sp}\, \underline{x} \tag{4.4}$$

where μ_{SP} is the short period frequency. Generally, the short period frequency is specified by handling qualities requirements and is not a parameter which can be altered during the loads controller design. Similarly, the coupling between the aircraft pitch rate and body axis vertical velocity, hence angle of attack, are selected based upon handling qualities criteria. Thus treating q, δW, and μ_{SP} as known quantities, one can write eqn. (4.3) in matrix form.

$$\begin{bmatrix} -0.16\, I_\beta \Omega & -209.59 \\ 0 & 0 \end{bmatrix} \begin{bmatrix} q \\ \delta W \end{bmatrix} = \begin{bmatrix} -0.16\mu_{sp} I_\beta \Omega & 0.8K_\beta & 0 & 133110 \\ 0.8K_\beta & 0.16\mu_{sp} I_\beta \Omega & 133110 & 0 \end{bmatrix} \begin{bmatrix} a_1 \\ b_1 \\ \theta_{1c} \\ \theta_{1s} \end{bmatrix} \tag{4.5}$$

$$M_{qw} = \left[M_{ab} \;\vdots\; M_{cs} \right] \begin{bmatrix} a_1 \\ b_1 \\ \hline \theta_{1c} \\ \theta_{1s} \end{bmatrix}$$

The equation written above is overdetermined in that there is no unique combination of rotor cyclic flapping and cyclic control angles which yields zero in-plane loads. Physically, however, the rotor control angles and blade flapping responses will not be independent for fixed values of pitch rate and vertical body axis velocity. An approximate relationship between the rotor flapping and cyclic control angles can be obtained through the quasi-static flapping assumption, wherein one assumes that the rotor flapping states reach a steady-state condition instantly.

The state vector can be partitioned into rigid body and flapping degrees of freedom, and the state equations rewritten in the form:

$$\begin{bmatrix} \dot{\underline{x}} \\ \hline \dot{\underline{\beta}} \end{bmatrix} = \left[\begin{array}{c|c} A_{11} & A_{12} \\ \hline A_{21} & A_{22} \end{array} \right] \begin{bmatrix} \underline{x} \\ \hline \underline{\beta} \end{bmatrix} + \begin{bmatrix} B_1 \\ \hline B_2 \end{bmatrix} \underline{u} \tag{4.6}$$

The quasi-static flapping approximation assumes that the time rates of change of the flapping states instantly approach zero, therefore:

$$\dot{\underline{\beta}} = 0 \tag{4.7}$$

The lower row of equations of eqn. (4.6) can then be solved algebraically, using the quasi-static flapping approximation, to give:

$$\underline{\beta} = -A_{22}^{-1} A_{21}\, \underline{x} - A_{22}^{-1} B_2\, \underline{u} \tag{4.8}$$

For the flight conditions considered in this analysis, the following relationship exists between rotor cyclic flapping angles and cyclic control angles, body axis velocity w, and pitch rate:

$$\begin{bmatrix} a_1 \\ b_1 \end{bmatrix} = M_L \begin{bmatrix} \theta_{1c} \\ \theta_{1s} \end{bmatrix} + M_R \begin{bmatrix} q \\ \delta W \end{bmatrix}$$

$$M_L = \begin{bmatrix} 0.84 & -1.45 \\ 1.46 & 0.82 \end{bmatrix} \quad M_R = \begin{bmatrix} 0.144 & -0.0016 \\ -0.0507 & 0.0008 \end{bmatrix} \tag{4.9}$$

The expressions above have been derived under the assumption that the flapping state variables instantly reach steady-state values. In actuality, some finite time interval will elapse before the flapping dynamics decay and the blade lateral and longitudinal flapping angles reach the steady-state values predicted by eqn. (4.9). The phase relationship between rotor cyclic control inputs and aircraft state can be better represented by remembering that the lowest frequency fixed-frame flapping mode occurs at a complex frequency of:

$$(\Omega - \omega_\beta) = -6.85 \pm 2.78j \quad \text{RAD/SEC}$$

The time to reach steady-state conditions of these low frequency flapping dynamics is given roughly by the inverse of the undamped natural frequency of the regressive flapping mode:

$$\tau = 0.135 \text{ SECONDS}$$

The desired short period frequency will be chosen as:

$$\mu_{sp} = -3 \pm 3j \quad \text{RAD/SEC}$$

Thus, if the effect of the flapping dynamics is represented by a pure time delay, the relationship between the rotor cyclic control inputs and aircraft pitch rate and vertical velocity states responding through the short period dynamics is given by:

$$\begin{bmatrix} a_1 \\ b_1 \end{bmatrix} = \left(M_L \begin{bmatrix} \theta_{1c} \\ \theta_{1s} \end{bmatrix} + M_R \begin{bmatrix} q \\ \delta W \end{bmatrix} \right) e^{-(3+3j)(-\tau)}$$

One can write the relationship between the cyclic flapping, rotor cyclic pitch, and aircraft rigid body states more succinctly as:

$$\begin{bmatrix} a_1 \\ b_1 \end{bmatrix} = M_L' \begin{bmatrix} \theta_{1c} \\ \theta_{1s} \end{bmatrix} + M_R' \begin{bmatrix} q \\ \delta W \end{bmatrix} \qquad (4.10)$$

where:

$$M_L' = e^{3\tau} \; e^{-3j\tau} \; M_L$$

$$M_R' = e^{3\tau} \; e^{-3j\tau} \; M_R$$

After substituting the above into eqn. (4.5), and performing some simple matrix algebra, one can solve for the desired θ_{1c} and θ_{1s} participation factors in terms of the specified pitch rate and body axis vertical velocity participation factors from:

$$\begin{bmatrix} \theta_{1c} \\ \theta_{1s} \end{bmatrix} = \left[M_{cs} + M_{ab} M_L' \right]^{-1} \left[M_{qw} - M_{ab} M_R' \right] \begin{bmatrix} q \\ \delta W \end{bmatrix} \qquad (4.11)$$

The desired lateral and longitudinal flapping participation factors can then be found from eqn. (4.10).

One can choose the desired closed-loop coning and airspeed participation factors to be equal to the open-loop values. The eigenvector which contains the desired coupling of the state variables is termed the "desired eigenvector". Table 4.1 compares the open-loop and desired short period eigenvectors for the tiltrotor in-plane loads reduction example. In reality, the physics of the system may make it impossible to use the available controls to achieve the form of the desired closed-loop eigenvector in an exact sense. An algorithm is described in the following sections which produces the controller which most closely approximates the desired eigenvector in a weighted least-squares sense.

4.3 Formulation of Closed-Loop Eigenvalue Problem

When a control of the form shown below is

$$\underline{u} = -G\underline{x} + \underline{v} \qquad (4.12)$$

used on the system of eqn. (4.1), the closed-loop state equations become:

$$\dot{\underline{x}} = [A - BG]\,\underline{x} + B\underline{v} \qquad (4.13)$$

The closed-loop eigenvalue problem can thus be formulated:

$$[\mu_i I - A + BG]\,\underline{p}_i = 0 \qquad (4.14)$$

or:

$$[\mu_i I - A]\,\underline{p}_i = -BG\,\underline{p}_i \qquad (4.15)$$

where μ_i is the closed-loop pole location and $\underline{p}_i$ is the associated closed-loop eigenvector. Now make the substitution:

$$\underline{q}_i = -G\,\underline{p}_i$$

$$[\mu_i I - A]\,\underline{p}_i = B\,\underline{q}_i \qquad (4.16)$$

and note that if μ_i is an open-loop eigenvalue of the system one can write:

$$[\mu_i I - A]\,\underline{p}_i = 0 \qquad (4.17)$$

$$B\,\underline{q}_i = 0$$

If the null space of B consists only of the zero vector, it is true that when the ith eigenvalue is invariant under feedback:

$$\underline{q}_i = 0 \qquad (4.18)$$

If μ_i is not an open-loop eigenvalue of the system one can write:

$$\underline{p}_i = [\mu_i I - A]^{-1} B\,\underline{q}_i \qquad (4.19)$$

Upon making the substitution:

$$M_i = [\mu_i I - A]^{-1} B \qquad (4.20)$$

one obtains:

$$\underline{p}_i = M_i\,\underline{q}_i \qquad (4.21)$$

4.4 Solving for the Achievable Eigenvectors

One would like to make the closed-loop eigenvector corresponding to the short period mode $\underline{p}_i$ equal to the desired eigenvector $\underline{v}_i$. One can express this desire in equation form as:

$$\underline{v}_i = M_i\,\underline{q}_i \qquad (4.22)$$

The equation will have a solution, which is not necessarily unique, only if:

$$\text{rank}\,[\,M_i \,|\, \underline{v}_i\,] = \text{rank}\,[\,M_i\,] \qquad (4.23)$$

For the tiltrotor aircraft and the chosen desired eigenvalues and eigenvectors, the rank condition above is not satisfied. As a result, a least-squares algorithm can be used to minimize the difference between the desired eigenvectors and the best achievable eigenvectors [21]. Therefore minimize the terms:

$$[\,\underline{v}_i - \underline{p}_i\,]$$

$$[\,\underline{v}_i - M_i\,\underline{q}_i\,] \qquad (4.24)$$

At this point, the eigenstructure assignment methodology used in this analysis departs from the methodology most often presented in the literature [15]. In the conventional approach, one partitions the state vector into two components. The first component consists of elements whose participation factors in the eigenvectors are specified, while the second component consists of elements whose participation factors remain unspecified during the design process. Only the difference between the specified elements of the achievable eigenvector and the specified elements of the desired eigenvector is minimized. Generally, only m elements of the eigenvector are specified, where m is the number of independent control surfaces, in order to provide an exact achievement of the specified portion of the desired eigenvector. In the conventional eigenstructure assignment approach, the designer is left with an equal amount of control over matching the response of each of the specified states in the system and no control over the unspecified state responses. In the approach presented here, a weighted least-squares approach is used to exercise some degree of control over matching each component of the achievable and desired eigenvectors.

The weighted least-squares eigenstructure assignment approach has several advantages over the conventional vector partitioning approach. First, the weighted least-squares technique gives the designer the ability to place varying degrees of emphasis on achieving each of the specified components of the eigenvector. In the tiltrotor loads example, the engineer may want to specify the pitch rate and cyclic flapping components of the eigenvector without drastically altering the aircraft angle of attack characteristics of the short period response. Trade studies can be performed, wherein loads are minimized at the expense of changing the aircraft response, by varying the relative weightings on the specified components of the eigenvector. Secondly, the weighted least-squares approach can be used to place some emphasis on retaining the open-loop characteristics of the unspecified elements of the eigenvector. In assigning the specified components of the eigenvector as closely as possible to the desired eigenvector components, the unspecified components of the eigenvector may be changed significantly, thereby completely altering the modal characteristics of the response. Weighting the difference between the open-loop and closed-loop unspecified components of the eigenvector can ensure that a weakly coupled unspecified state, manifesting itself by a small relative participation factor in the open-loop eigenvector, is not used excessively to alter the specified participation factors in the controller design.

The component weightings used to place varying degrees of emphasis on minimizing the components of the vector of eqn. (4.24) are weightings of 100 on the pitch rate and longitudinal and lateral flapping angle and rate states, and weightings of unity on all other states in the system. The solution to the weighted least-squares problem is given by:

$$\underline{g}_i = (M_i^T W_i M_i)^{-1} M_i^T W_i \underline{v}_i \tag{4.25}$$

where W_i are diagonal weighting matrices, corresponding to each mode in the system, which specify the relative emphasis placed upon achieving each component of the desired eigenvectors. Remembering eqn. (4.22), the best achievable eigenvectors are given by:

$$\underline{p}_i = M_i \underline{g}_i \tag{4.26}$$

Table 4.2 compares the desired and achievable short period eigenvectors for the tiltrotor loads minimization problem.

4.5 Finding the Feedback Gains

Remembering the definition of eqn. (4.16), one can construct the matrix equation:

$$\begin{aligned} Q &= -GP \\ Q &= [\, \underline{g}_1 \mid \underline{g}_2 \mid \cdots \underline{g}_n \,] \\ P &= [\, \underline{p}_1 \mid \underline{p}_2 \mid \cdots \underline{p}_n \,] \end{aligned} \tag{4.27}$$

The achievable closed-loop eigenvectors p_i are linearly independent, therefore one can solve for the gains from:

$$G = -QP^{-1} \tag{4.28}$$

The gain matrix above is an array of feedback gains from each state in the system to each available control surface. This type of control law is known as a "full state feedback" design. For example, in the case where actuator dynamics exist in the math model, a full state feedback controller senses actuator rates and displacements and feeds back proportional signals to the actuator inputs. A variety of reasons, including sensor noise, unmodelled dynamics, or processing delays, may preclude the feedback of certain dynamic states in the system.

A controller design which does not utilize all the system states is referred to as a "constrained state feedback" design. Eliminating a given state from the feedback signal is equivalent to equating a column of the gain matrix arbitrarily to zero. When the ith system state is suppressed in the feedback law, eqn. (4.27) can be written:

$$Q = -G'P' \tag{4.29}$$

where the matrix G' is the matrix G with the ith column deleted, while the matrix P' is the matrix P with the ith row deleted. The system of eqn (4.29) can be solved using a weighted least-squares algorithm in the following manner. Transpose both sides of eqn (4.29) to obtain:

$$Q^T = -(P')^T (G')^T \tag{4.30}$$

The weighted least-squares solution of the above is given by:

$$(G')^T = -[\, P' W_g (P')^T \,]^{-1} P' W_g Q^T \tag{4.31}$$

The constrained state feedback gain matrix is therefore given by:

$$G' = -Q W_g (P')^T [P' W_g (P')^T]^{-T} \tag{4.32}$$

Unfortunately, when the equation above contains complex mode shapes, corresponding to oscillatory modes, the gain matrix which best satisfies the least-squares problem may also be complex. One can find the real matrix $(G')^T$ which best satisfies eqn. (4.29) by considering the complex conjugate pair rows of eqn. (4.29):

$$\begin{aligned} \underline{g}_i^T &= -(\underline{p}_i')^T (G')^T \\ (\underline{g}_i^*)^T &= -(\underline{p}_i'^*)^T (G')^T \end{aligned} \tag{4.33}$$

First adding the two equations above, and then subtracting the lower equation from the upper equation yields:

$$\begin{aligned} \text{real}\, [\underline{g}_i^T] &= -\,\text{real}\, [(\underline{p}_i')^T]\, (G')^T \\ \text{imag}\, [\underline{g}_i^T] &= -\,\text{imag}\, [(\underline{p}_i')^T]\, (G')^T \end{aligned} \tag{4.34}$$

This procedure can be repeated for each complex conjugate pair of eigenvectors in the system to obtain a reformulated version of eqn. (4.29), in which both the Q' and P' matrices are real valued. The resulting constrained state feedback gain matrix G', which best satisfies the weighted least-squares problem, will also be real valued.

The weighting matrix in the constrained state feedback design represents the relative degree of emphasis placed upon matching each desired eigenvector in the system. In general, it is not possible to replicate the closed-loop eigenstructure produced by a state feedback design by the more restrictive constrained state feedback controller. As a result, in order to closely match any particular desired eigenvector, the designer must accept some degree of variation in the other eigenvectors caused by differences in the full state feedback and constrained state feedback controllers. It should also be noted that the constrained state feedback controller places the desired eigenvalues in only an approximate sense, whereas the full state feedback controller has the ability to place exactly the desired eigenvalues. The short period eigenvectors were weighted extremely heavily (100:1) in relation to all other eigenvectors in the constrained state feedback controller design.

Presented in Table 4.3 are the feedback gains which produce the achievable short period eigenvector. Shown in Fig. 4.1 are the closed-loop longitudinal step responses for the eigenstructure assignment based controller. In comparison to Fig. 3.5, one can observe that the pitch rate, angle of attack, and vertical acceleration reponses are unchanged, while the in-plane loads are reduced. Figure 4.2 presents a direct comparison of the cumulative in-plane moments, defined as the square root of the sum of the squares of the sine and cosine components of the in-plane moments, for the ref. [1] type controller and the controller which utilizes rotor cyclic pitch inputs. It is apparent that, using both rotor cyclic pitch and elevator inputs, eigenstructure assignment can be used to design an effective in-plane loads controller.

5. The Rotor In-Plane Moment Controller

5.1 Introduction

In the previous chapter, the eigenstructure assignment methodology was demonstrated by designing a controller which minimized the in-plane rotor loads encountered during the short period dynamics of the aircraft. The design has not yet been optimized to give acceptable long term performance, nor has any consideration been given to the control authorities required to minimize the loads. In the following sections, the eigenstructure assignment design procedure will be extended to the longer term dynamics of the aircraft through proper shaping of the closed-loop phugoid eigenvector. In addition, the control usage of the in-plane load controller will be constrained to remain within the authority limits of the rotor cyclic pitch controls for pitch rates of up to fifty degrees per second.

5.2 Consideration of Cyclic Pitch Authority Limits

The optimal short period in-plane load controller designed in chapter 4 uses roughly .385 degrees of longitudinal cyclic pitch control for each degree per second of aircraft pitch rate. At the .385 deg/(deg/sec) rate of control usage, the ten degree longitudinal cyclic authority will be saturated at a pitch rate of 26 deg/sec. In order to retain controller effectiveness for pitch rates up to 50 deg/sec, the control usage per unit pitch rate must be halved.

Remembering that the longitudinal cyclic pitch angles are included as dynamic states in the math model, one can limit the control usage by halving the longitudinal and lateral cyclic control angle participation factors in the desired short period eigenvector. Application of the eigenstructure assignment methodology discussed in chapter 4 produces the closed-loop responses shown in Figure 5.1. The limited authority controller sacrifices performance, in the form of higher in-plane moments, for an increase in the range of pitch rate over which there is a reduction in rotor loads. The limited authority controller can produce a 50% reduction in in-plane moments for pitch rates up to 50 deg/sec.

5.3 Design of Phugoid Eigenvector

In order to understand the interaction between the short period and phugoid mode dynamics of the aircraft, consider again the pull-up maneuver shown in Figure 3.3. The longitudinal stick step first produces aircraft pitch rate, which then quickly is integrated to a significant Euler pitch angle in the first second of the maneuver. The increase in pitch angle leads to a component of the aircraft forward velocity along the vertical body axis of the aircraft.

The short period dynamics decay within two seconds of the initiation of the maneuver, leaving the body axis vertical velocity as a virtual initial condition as seen by the phugoid mode. The body axis velocity δW produces an increase in the lift force exerted on the aircraft, engendering an inertial axis vertical acceleration which eventually results in a steady state rate of climb. After a period of ten seconds, the aircraft rate of climb almost cancels the component of the relative wind projected on the body vertical axis, and the relative wind is once again aligned with the body longitudinal axis.

When the in-plane loads controller is designed to alter only the short period dynamics of the aircraft, the step control input results in feedback signals which remain constant after the conclusion of the short period dynamics. The rotor cyclic pitch angles will retain some steady state value, causing steady state rotor cyclic flapping after the completion of the maneuver. The presence of steady state cyclic flapping will produce unnecessary aerodynamic one/rev moments on the rotor blades which oppose the hub moments exerted by the gimbal spring restraint. As a result, it is desirable to return the rotor to the initial operating conditions of zero cyclic pitch control and zero cyclic flapping through the phugoid dynamics of the aircraft.

At the completion of the short period dynamics excited by the pull-up maneuver, when the aircraft pitch rate and rotor flapping rates are essentially zero, the in-plane moments are given approximately by:

$$\delta M_H = \{0.8K_\beta\, b_1 + 133110\ \theta_{1S} + 209.59\ \delta W\} \sin\varphi \qquad (5.1)$$

$$+ \{0.8K_\beta\, a_1 + 133110\ \theta_{1C}\} \cos\varphi$$

The body axis velocity δW is at this time decaying through the phugoid dynamics of the aircraft, while the cyclic pitch terms remain constant. In order to drive the rotor cyclic pitch controls back to the neutral positon, while retaining low in-plane moments through the latter phase of the maneuver, it is desirable to dynamically couple the rotor cyclic pitch and δW velocity pertubations during the phugoid dynamics. In this way, the inital rotor cyclic pitch angles will be seen as an initial condition, in analogy to the body axis vertical velocity, which will be eliminated through the phugoid dynamics.

One can select the coupling between the states in the equation above to minimize the long term in-plane moments through shaping the phugoid eigenvector in a similar manner to that developed for the short period eigenvector in chapter 4. The desired phugoid eigenvalue can be placed arbitrarily close to the open-loop phugoid pole. The resulting desired phugoid eigenvector can then be incorporated into the eigenstructure assignment controller design process. Table 5.1 presents the finalized closed-loop short period and phugoid eigenvectors. Shown in Fig. 5.2 are the time histories of the aircraft responses to a longitudinal stick step input, demonstrating the long-term performance of the in-plane load controller.

5.4 Controller Evaluation

The feedback gains developed for the finalized in-plane load controller are given in Table 5.2, while the closed-loop pole locations are detailed in Table 5.3. The effect of the load controller on the cumulative in-plane moment is illustrated in Fig. 5.3, wherein the open-loop, elevator-only, and combined rotor cyclic pitch and elevator controllers are compared for longitudinal stick step inputs. It should be remembered that almost identical pitch rate responses are produced by the elevator-only and combined elevator and cyclic pitch controllers, while the in-plane loads are halved by the introduction of active rotor cyclic pitch control.

The robustness properties of the controller can be demonstrated by the use of the stability robustness tests developed by Lehtomahki [10]. When modelling errors are represented as a multiplicative error at the plant input, one can show that the resulting controller will be stable in the presence of the worst modelling error by conducting the following singular value test. Stability is ensured if the maximum singular value of the closed-loop transfer function matrix, relating the closed-loop feedback signal to the elevator and cyclic pitch controls, is less than the inverse of the maximum singular value of the multiplicative modelling error at all frequencies. Essentially, the stability robustness criterion dictates that the bandwidth of the controller be limited to the frequency range where the mathematical model of the plant has high fidelity.

In this analysis, modelling uncertainty is mainly a result of neglecting the in-plane rotor dynamics. The lowest natural frequency of the in-plane dynamics occurs at approximately twenty rad/sec, therefore the maximum singular value of the closed-loop feedback transfer function matrix should crossover well before twenty rad/sec. Figure 5.4 shows that crossover occurs well below the rotor in-plane natural frequencies, as a result the controller is ensured stability in the presence of lead-lag dynamics.

The eigenstructure assignment methodology should produce a reduction in the in-plane loads for all input forcing frequencies which excite the short period and phugoid modes. Shown in Fig. 5.5 is the Bode magnitude plot of the sine component of the in-plane loads, produced as a function of longitudinal stick input frequency, for the elevator-only and combined elevator and cyclic pitch controllers. Throughout the range of possible pilot input frequencies, which occur below two hertz, the in-plane loads frequency response produced by the combined elevator and cyclic pitch controller is roughly six decibels less than that engendered by the elevator-only controller. At high frequencies controller effectiveness decreases, in keeping with the stability robustness constraint, and the combined cyclic pitch and elevator and elevator-only controllers result in effectively the same loads.

It is interesting to consider the effect of the rotor flapping state feedback gains on control system performance. Although methods exist to obtain accurate measurements of the rotor flapping states [6], the elimination of these feedbacks is beneficial from the standpoint of simplified controller implementation. Setting the rotor state feedback terms to zero causes a negligible difference in aircraft and in-plane loads responses in comparison to the full element controller results shown in Fig. 5.2. Similarly, the frequency response characteristics of the controller, from both performance and stability robustness perspectives, are unaltered by eliminating the rotor state feedbacks from the controller design.

6. Conclusions

A combined cyclic pitch and elevator controller has been developed which can reduce rotor in-plane loads by fifty percent in comparison to existing controller designs. The controller has been designed to compensate for the effect of realistic actuator dynamics, while exhibiting robustness to high frequency modelling errors. The optimal controller design includes feedback of the rotor flapping states, however, elimination of the rotor state feedback in the interest of reduced controller complexity results in very little degradation in loads alleviation capability.

The in-plane loads controller primarily utilizes constant gain feedback of pitch rate, Euler pitch angle, and body axis vertical velocity to rotor lateral and longitudinal cyclic pitch angles. Active rotor cyclic pitch changes are appropriately phased with aircraft pitch rate and angle of attack changes, thereby eliminating the tendency of the rotor tip-path-plane to lead the mast during precession. When the aircraft attains peak pitch rates, controller inputs produce a flapping response which precesses the tip-path-plane in an opposite direction to the mast angular pitch rate. The resulting maximum total rotor angular rate, defined as the sum of aircraft pitch rate and longitudinal flapping rate, is reduced, thereby alleviating the aerodynamic moments which must exist in order to precess the rotor. Also, rotor cyclic pitch is used to exert in-plane aerodynamic forces on the blade, partially cancelling the in-plane forces engendered by the out-of-plane precessional moments.

Eigenstructure assignment methodology has been used to incorporate realistic controller authority limits into the controller design process. The ten degree longitudinal cyclic pitch authority of the controller is not exceeded when pitch rate is less than fifty degrees per second. Flapping motion during aggressive pitch axis maneuvers is reduced in comparison to the fixed cyclic pitch configuration, thus the risk of rotor/airframe interference is lowered.

References

1) Schillings, J. et. al., "Maneuver Performance of Tiltrotor Aircraft", 43rd Annual National Forum of the American Helicopter Society, May 1987.

2) Van Gaasbeek, J. R., "Rotorcraft Flight Simulation Computer Program C81 with Data Map Interface", USAAVRADCOM TR-80-D-38A, Users Manual, October 1981.

3) Batra, N. N., Marr, R. L., and Joglekar, M. M., "A Generic Simulation Model for Tiltrotor Aircraft", Bell-Boeing Technical Report 901-909-003, November 1985.

4) Kolk, Richard W., "Modern Flight Dynamics", Prentice-Hall Inc., 1961.

5) Straub, F. K. and Warmbrodt, W., "The Use of Active Controls to Augment Rotor/Fuselage Stability", Journal of the American Helicopter Society, July 1985.

6) Ham, N. D., Balough D. L., and Talbot, P. D., "The Measurement and Control of Helicopter Blade Modal Response Using Blade-Mounted Accelerometers", Thirteenth European Rotorcraft Forum, Paper No. 6-10, September 1987.

7) Coleman, Robert P., and Feingold, Arnold M., "Theory of Self Excited Mechanical Oscillations of Helicopter Rotors with Hinged Blades", NACA Report 1351, 1958.

8) Ham, N. D., "Helicopter Individual-Blade-Control Research at MIT 1977-1985", Vertica, 11, No. 1/2, pp. 109-122, 1987.

9) McKillip, R. M., Jr., "Periodic Control of the Individual-Blade-Control Helicopter Rotor", Vertica, 9, pp. 199-224, 1985.

10) Lehtomaki, N. A., Sandell, N. S., and Athans, M., "Robustness Results in Linear-Quadratic Gaussian Based Multivariable Control Designs", IEEE Transactions on Automatic Control, Vol. AC-26, No. 1, February 1981.

11) Athans, M. et. al., "Linear-Quadratic Gaussian with Loop-Transfer Recovery Methodology for the F-100 Engine", Journal of Guidance, Control, and Dynamics, Vol. 9, No. 1, Jan.-Feb. 1986.

12) Francis, B. A., "A Course in H-Infinity Control Theory", Springer Verlag, 1987.

13) Yue, Andrew and Postlethwaite, Ian, "H-Infinity Design and the Improvement of Helicopter Handling Qualities", Thirteenth European Rotorcraft Forum, Paper No. 7.2, September 1987.

14) Kalman, R. E., "When is a Linear Control System Optimal?", Trans. ASME Ser. D:J. Basic Eng, Vol. 86, pp. 51-60, March 1964.

15) Andry, A. N., Jr., Shapiro, E. Y. and Chung, J.C., "Eigenstructure Assignment for Linear Systems", *IEEE Transactions on Aerospace and Electronic Systems*, Vol. AES-19, No. 5, September 1983.

16) Etkin, B., "Dynamics of Flight-Stability and Control", John Wiley and Sons, 1982.

17) Symbolics, Inc., "VAX UNIX MACSYMA Reference Manual", Document No. SM10501030.011, November 1985.

18) Gibbons, M. P. and Done, G. T. S., "Automatic Generation of Helicopter Rotor Aeroelastic Equations of Motion", Proceedings of the Eighth European Rotorcraft Forum, Paper No. 33, August 31, 1982.

19) Miller, D. G. and White, F., "A Treatment of the Impact of Rotor/Fuselage Coupling on Helicopter Handling Qualities", 43rd Annual National Forum of the American Helicopter Society, May 1987.

20) Popelka, D., Sheffler, M., and Bilger, J., "Correlation of Test and Analysis for the 1/5-Scale V-22 Aeroelastic Model", Journal of the American Helicopter Society, April 1987.

21) Moore, B. C., "On the Flexibility Offered by State Feedback in Multivariable Systems Beyond Closed-Loop Eigenvalues", Proceedings of the 14th IEEE Conference on Decision and Control, Houston, Texas, December 1975.

MODE	FREQUENCY (rad/sec)
Symmetric Progressive Flap.	-6.5 + 72.8i
Antisymmetric Progressive Flap.	-6.5 + 72.8i
Symmetric Coning	-6.4 + 40.7i
Antisymmetric Coning	-6.3 + 41.5i
Symmetric Regressive Flap.	-7.0 + 2.8i
Antisymmetric Regressive Flap.	-6.9 + 2.8i
Short Period	-1.5 + 2.3i
Roll Convergence	-1.7003
Dutch Roll	-0.2 + 1.5i
Phugoid	-0.1 + 0.2i
Spiral	-0.0569
Heading	0.0000
Integral Longitudinal Velocity	0.0000
Integral Vertical Velocity	0.0000
Elevator Actuator	-20.000
Right Rotor Long. Cyclic Pitch Act.	-20.000
Right Rotor Lat. Cyclic Pitch Act.	-20.000
Left Rotor Long. Cyclic Pitch Act.	-20.000
Left Rotor Lat. Cyclic Pitch Act.	-20.000

Table 2-I: Tiltrotor Open-Loop Modes at 260 Knots

NUMBER	STATE	UNITS
1	Elevator Deflection	in
2	Rt. Rotor Lat. Cyc. Pitch	deg
3	Rt. Rotor Long. Cyc. Pitch	deg
4	Lt. Rotor Lat. Cyc. Pitch	deg
5	Lt. Rotor Long. Cyc. Pitch	deg
6	Airspeed	ft/sec
7	Lateral Velocity	ft/sec
8	Vertical Velocity	ft/sec
9	Roll Rate	rad/sec
10	Pitch Rate	rad/sec
11	Yaw Rate	rad/sec
12	Pitch Angle	rad
13	Roll Angle	rad
14	Integral Vertical Velocity	ft
15	Heading Angle	rad
16	Integral Long. Velocity	ft
17	Integral Lat. Velocity	ft
18	Rt. Rot. Coning	rad
19	Rt. Rot. Long. Cyc. Flap	rad
20	Rt. Rot. Lat. Cyc. Flap	rad
21	Lt. Rot. Coning	rad
22	Lt. Rot. Long. Cyc. Flap	rad
23	Lt. Rot. Lat. Cyc. Flap	rad
24	Rt. Rot. Coning Rate	rad/sec
25	Rt. Rot. Long. Cyc. Flap Rate	rad/sec
26	Rt. Rot. Lat. Cyc. Flap Rate	rad/sec
27	Lt. Rot. Coning Rate	rad/sec
28	Lt. Rot. Long. Cyc. Flap Rate	rad/sec
29	Lt. Rot. Lat. Cyc. Flap Rate	rad/sec

Table 2-II: Description of Simulation State Variables

STATE	PARTICIPATION FACTOR OPEN-LOOP	DESIRED
1	0.00 + 0.00i	2.78 - .06i
2	0.00 + 0.00i	0.29 + 2.57i
3	0.00 + 0.00i	-16.22 - 21.78i
4	0.00 + 0.00i	0.29 + 2.57i
5	0.00 + 0.00i	-16.22 - 21.78i
6	-2.21 - 0.45i	-0.40 - 0.69i
7	-0.00 - 0.00i	-0.00 - 0.00i
8	-32.15 - 176.28i	-65.19 - 98.11i
9	-0.00 + 0.00i	-0.00 + 0.00i
10	1.00 + 0.00i	1.00 + 0.00i
11	0.00 + 0.00i	-0.00 + 0.00i
12	-0.20 - 0.31i	-0.17 - 0.17i
13	0.00 + 0.00i	0.00 - 0.00i
14	-47.91+45.33i	-5.49 + 27.22i
15	0.00 - 0.00i	0.00 - 0.00i
16	0.31 + 0.77i	-0.05 + 0.18i
17	0.00 + 0.00i	0.00 + 0.00i
18	-0.00 - 0.02i	0.00 - 0.00i
19	0.31 + 0.26i	-0.25 - 0.25i
20	-0.18 - 0.09i	0.06 - 0.15i
21	-0.00 - 0.02i	0.00 - 0.00i
22	0.31 + 0.26i	-0.25 - 0.25i
23	-0.18 - 0.09i	0.06 - 0.15i
24	0.06 + 0.03i	0.00 + 0.01i
25	-1.06 + 0.31i	1.49 - 0.02i
26	0.48 - 0.29i	0.28 + 0.62i
27	0.06 + 0.03i	0.00 + 0.01i
28	-1.06 + 0.31i	1.49 - 0.02i
29	0.48 - 0.29i	0.28 + 0.62i

Table 4-I: Open-Loop and Desired Short Period Eigenvectors for In-Plane Loads Reduction

STATE	PARTICIPATION FACTOR DESIRED	ACHIEVABLE
1	2.78 - .06i	3.03 - 0.21i
2	0.29 + 2.57i	0.31 + 2.69i
3	-16.22 - 21.78i	-16.45 - 21.73i
4	0.29 + 2.57i	0.31 + 2.69i
5	-16.22 - 21.78i	-16.45 - 21.73i
6	-0.40 - 0.69i	-0.48 - 0.51i
7	-0.00 - 0.00i	-0.00 - 0.00i
8	-65.19 - 98.11i	-64.30 - 96.56i
9	-0.00 + 0.00i	-0.00 - 0.00i
10	1.00 + 0.00i	1.00 + 0.00i
11	-0.00 + 0.00i	-0.00 + 0.00i
12	-0.17 - 0.17i	-0.17 - 0.17i
13	0.00 - 0.00i	0.00 + 0.00i
14	-5.49 + 27.22i	-5.38 + 26.81i
15	0.00 - 0.00i	0.00 + 0.00i
16	-0.05 + 0.18i	-0.01 + 0.16i
17	0.00 + 0.00i	0.00 + 0.00i
18	0.00 - 0.00i	0.00 - 0.00i
19	-0.25 - 0.25i	-0.15 - 0.20i
20	0.06 - 0.15i	0.15 - 0.01i
21	0.00 - 0.00i	0.00 - 0.00i
22	-0.25 - 0.25i	-0.15 - 0.20i
23	0.06 - 0.15i	0.15 - 0.01i
24	0.00 + 0.01i	0.01 + 0.01i
25	1.49 - 0.02i	1.05 + 0.15i
26	0.28 + 0.62i	-0.42 + 0.50i
27	0.00 + 0.01i	0.01 + 0.01i
28	1.49 - 0.02i	1.05 + 0.15i
29	0.28 + 0.62i	-0.42 + 0.50i

Table 4-II: Desired and Achievable Short Period Eigenvectors for In-Plane Loads Reduction

STATE	ELEV. (in)	RT. LAT. CYC. (deg)	RT. LONG. CYC. (deg)	LT. LAT. CYC. (deg)	LT. LONG. CYC. (deg)
1	0	0	0	0	0
2	0	0	0	0	0
3	0	0	0	0	0
4	0	0	0	0	0
5	0	0	0	0	0
6	-0.0005	0.0116	-0.1009	0.0116	-0.1009
7	0	0	0	0	0
8	0.0029	-0.01240	0.1181	-0.0124	0.1181
9	0	0	-0.0001	0	-0.0001
10	-1.2053	-0.8659	1.8240	-0.8659	1.8240
11	0.0001	0.0001	-0.0002	0.0001	-0.0002
12	-0.0528	0.1317	-1.5241	0.1317	-1.5241
13	0.0001	0	-0.0001	0	-0.0001
14	0	0	0	0	0
15	0	0	0	0	0
16	0	0	0	0	0
17	0	0	0	0	0
18	0.0670	0.1162	-0.6766	0.1162	-0.6766
19	-0.3305	-0.0032	-1.4783	-0.0032	-1.4783
20	-0.0499	0.0841	-0.9376	0.0841	-0.9376
21	0.0670	0.1162	-0.6767	0.1162	-0.6767
22	-0.3305	-0.0032	-1.4784	-0.0032	-1.4784
23	-0.0499	0.0841	-0.9375	0.0841	-0.9375
24	0.0112	0.0103	-0.0363	0.0103	-0.0363
25	0.0005	0.0021	-0.0154	0.0021	-0.0154
26	0.0047	0.0004	0.0181	0.0004	0.0181
27	0.0112	0.0103	-0.0363	0.0103	-0.0363
28	0.0005	0.0021	-0.0154	0.0021	-0.0154
29	0.0047	0.0004	0.0182	0.0004	0.1082

Table 4-III: Feedback Gains for In-Plane Loads Minimization

STATE	PARTICIPATION FACTOR PHUGOID	SHORT PERIOD
1	-0.00 + 0.00i	2.62 - 0.08i
2	0.00 + 0.00i	0.00 + 0.00i
3	0.10 + 0.01i	-6.78 - 10.46i
4	0.00 + 0.00i	0.00 + 0.00i
5	0.10 + 0.01i	-6.78 - 10.46i
6	1.00 + 0.00i	-0.40 - 0.69i
7	-0.00 + 0.00i	-0.00 - 0.00i
8	0.77 + 0.07i	-65.19 - 98.11i
9	0.00 + 0.00i	-0.00 + 0.00i
10	0.00 - 0.00i	1.00 + 0.00i
11	0.00 + 0.00i	-0.00 + 0.00i
12	-0.00 + 0.01i	-0.17 - 0.17i
13	-0.00 + 0.00i	0.00 - 0.00i
14	-1.64 + 2.47i	-5.49 + 27.22i
15	-0.00 - 0.00i	0.00 - 0.00i
16	-1.80 + 3.36i	-0.05 + 0.18i
17	0.00 - 0.00i	0.00 + 0.00i
18	-0.00 + 0.00i	0.00 + 0.00i
19	-0.00 - 0.00i	-0.25 - 0.25i
20	0.00 + 0.00i	0.06 - 0.15i
21	-0.00 + 0.00i	0.00 - 0.00i
22	-0.00 - 0.00i	-0.25 - 0.25i
23	0.00 + 0.00i	0.06 - 0.15i
24	0.00 + 0.00i	0.00 + 0.01i
25	0.00 + 0.00i	1.49 - 0.02i
26	-0.00 - 0.00i	0.28 + 0.62i
27	0.00 + 0.00i	0.00 + 0.02i
28	0.00 + 0.00i	1.49 - 0.02i
29	0.00 + 0.00i	0.28 + 0.62i

Table 5-I: Finalized Closed-Loop Short Period and Phugoid Eigenvectors

STATE	ELEV. (in)	RT. LAT. CYC. (deg)	RT. LONG. CYC. (deg)	LT. LAT. CYC. (deg)	LT. LONG CYC. (deg)
1	0	0	0	0	0
2	0.	0	0	0	0
3	0	0	0	0	0
4	0	0	0	0	0
5	0	0	0	0	0
6	0.0107	0.0011	0.0030	0.0011	0.0030
7	0	0	0	0	0
8	-0.0029	-0.0010	0.0551	-0.0010	0.0551
9	0	0	-0.0001	0	0.0001
10	-1.3827	-0.0915	1.3025	-0.0915	1.3026
11	0.0001	0.0000	-0.0001	0.0000	0.0001
12	0.1660	0.0128	0.0309	0.0128	0.0309
13	0.0001	0	-0.0001	0	-0.0001
14	0	0	0	0	0
15	0	0	0	0	0
16	0	0	0	0	0
17	0	0	0	0	0
18	0.1149	0.0108	-0.2715	0.0108	-0.2715
19	-0.2825	-0.0061	-0.6159	-0.0061	-0.6159
20	-0.0080	0.0059	-0.4466	0.0059	-0.4466
21	0.1150	0.0108	-0.2715	0.0108	-0.2715
22	-0.2825	-0.0061	-0.6159	-0.0061	-0.6159
23	-0.0080	0.0059	-0.4465	0.0059	-0.4465
24	0.0150	0.0011	-0.0118	0.0011	-0.0118
25	0.0013	0.0002	-0.0077	0.0002	-0.0077
26	0.0041	0.0001	0.0073	0.0001	0.0073
27	0.0150	0.0011	-0.0118	0.0011	-0.0118
28	0.0013	0.0002	-0.0077	0.0002	-0.0077
29	0.0041	0.0001	0.0073	0.0001	0.0073

Table 5-II: Finalized In-Plane Loads Controller Feedback Gains

MODE	FREQUENCY
Symmetric Progressive Flap.	-6.5 + 72.8i
Antisymmetric Progressive Flap.	-6.5 + 72.8i
Symmetric Coning	-6.4 + 40.7i
Antisymmetric Coning	-6.3 + 41.5i
Symmetric Regressive Flap.	-7.0 + 2.8i
Antisymmetric Regressive Flap.	-6.9 + 2.8i
Short Period	-3.0 + 3.0i
Roll Convergence	-1.7003
Dutch Roll	-0.2 + 1.5i
Phugoid	-0.1 + 0.2i
Spiral	-0.0569
Heading	0.0000
Integral Longitudinal Velocity	0.0000
Integral Vertical Velocity	0.0000
Elevator Actuator	-15.099
Out-Of-Phase Long. Cyc. Pitch Act.	-20.000
In-Phase Long. Cyc. Pitch Act.	-19.558
In-Phase Lat. Cyc. Pitch Act.	-20.000
Out-Of-Phase Lat. Cyc. Pitch Act.	-20.000

Table 5-III: Finalized Closed-Loop Eigenvalues

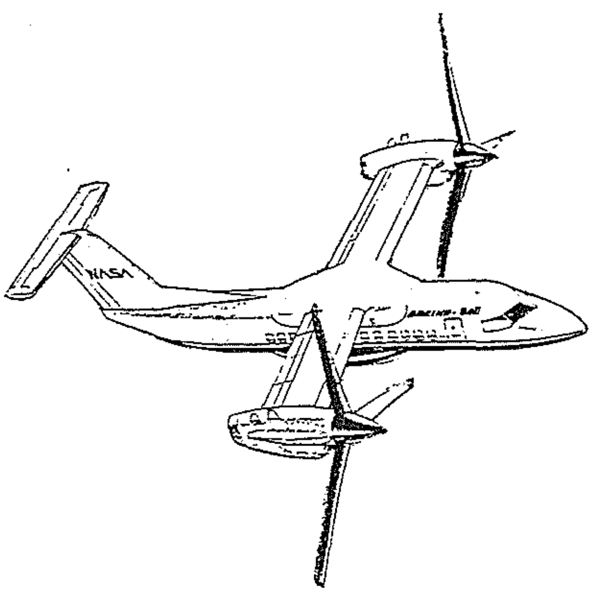

Figure 1-1: Artist's Conception of Commercial Tiltrotor

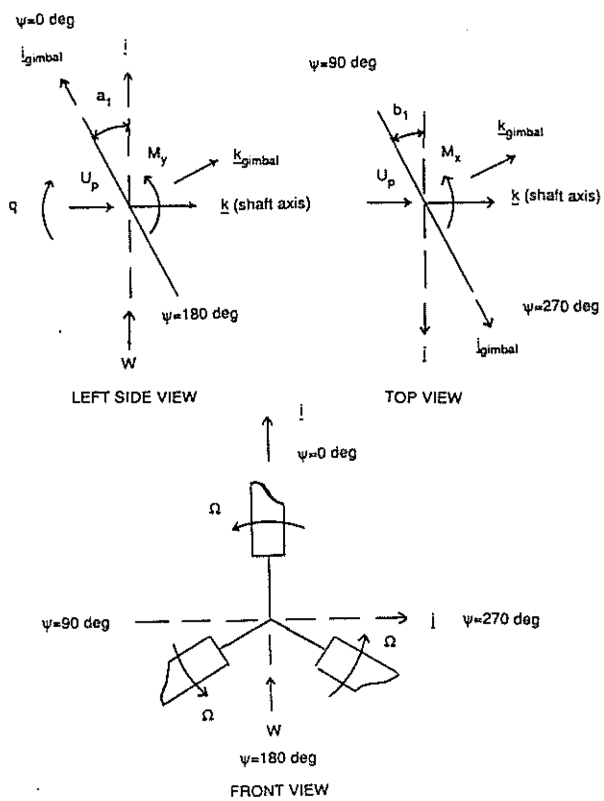

Figure 3-1: Gimbal Axis System

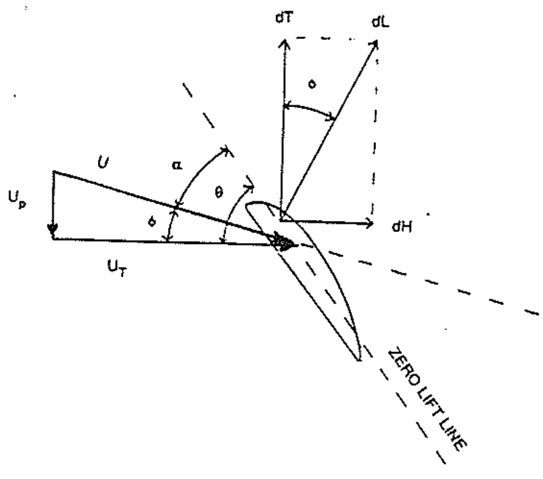

Figure 3-2: Relative Wind And Airfoil Geometry

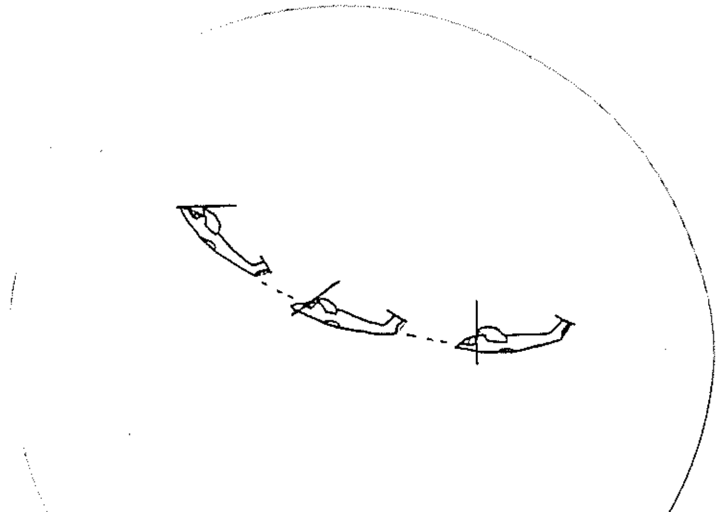

Figure 3-4: Rotor Flapping Responses During Tiltrotor High Speed Pull-Up Maneuver

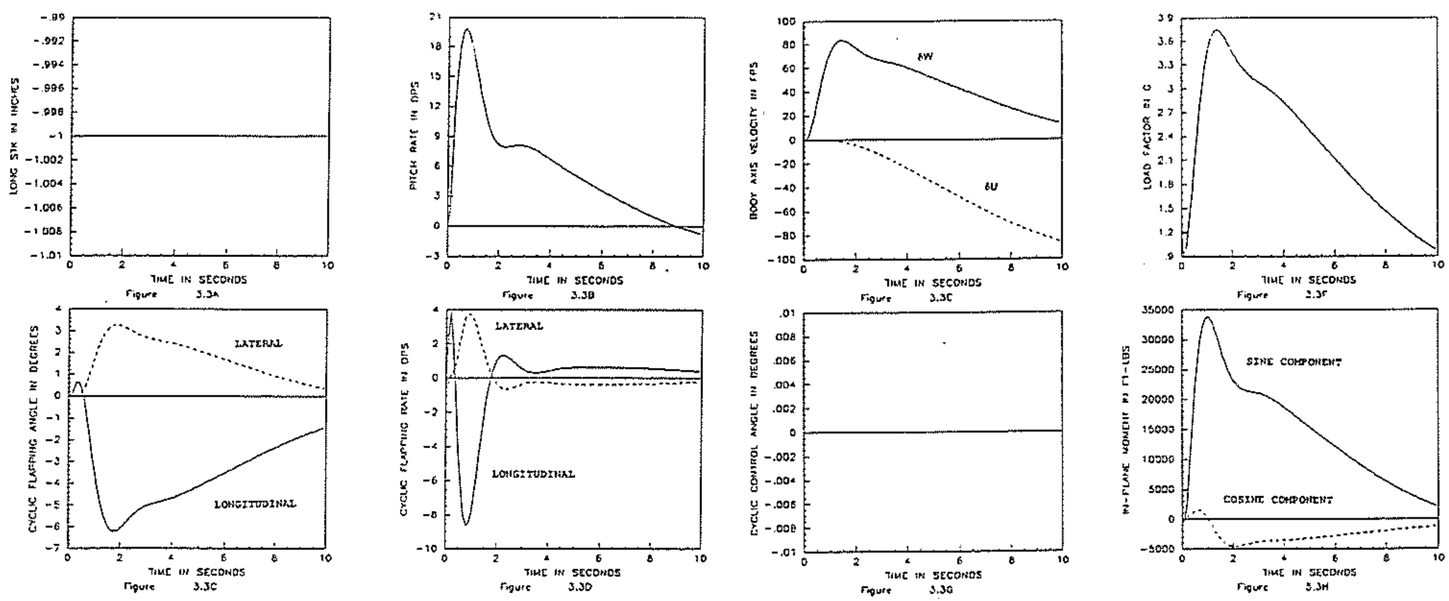

Figure 3-3: Open-Loop Longitudinal Stick Step Responses

Figure 3-3
, continued

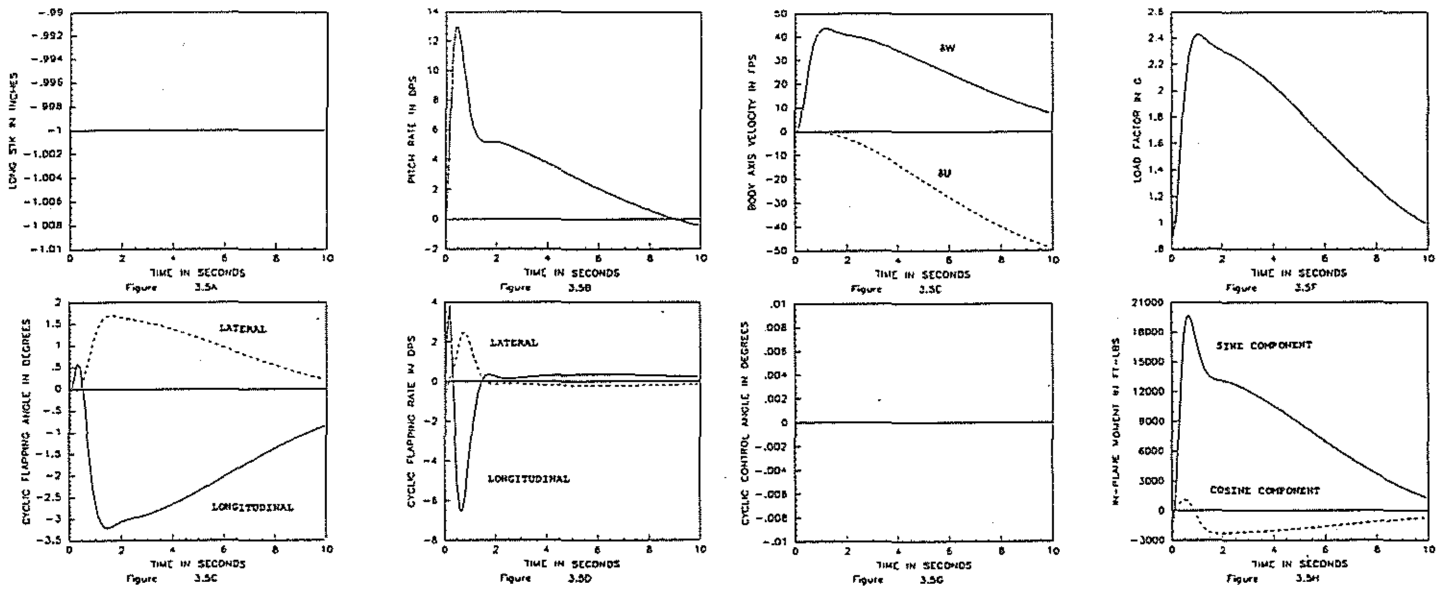

Figure 3-5: Longitudinal Stick Step Responses for Pitch Rate to Elevator Feedback Controller

Figure 3-5, continued

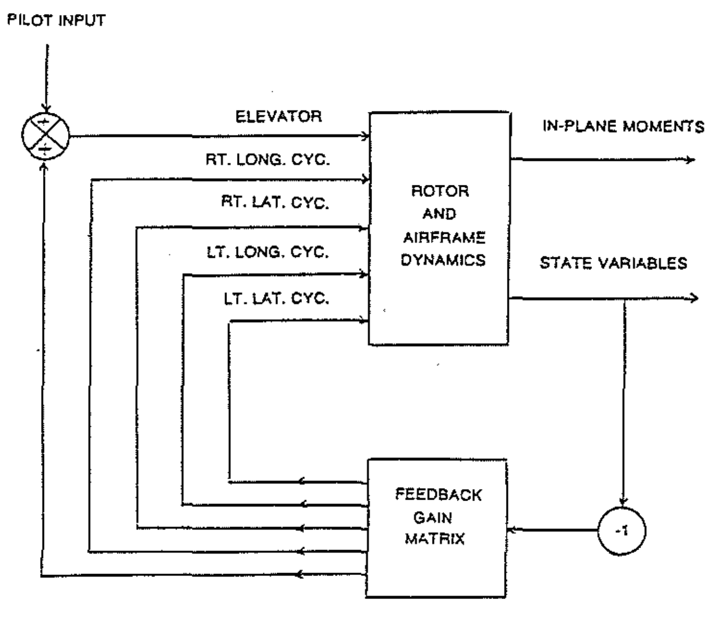

Figure 3-6: Block Diagram of Combined Elevator and Rotor Cyclic Pitch Controller

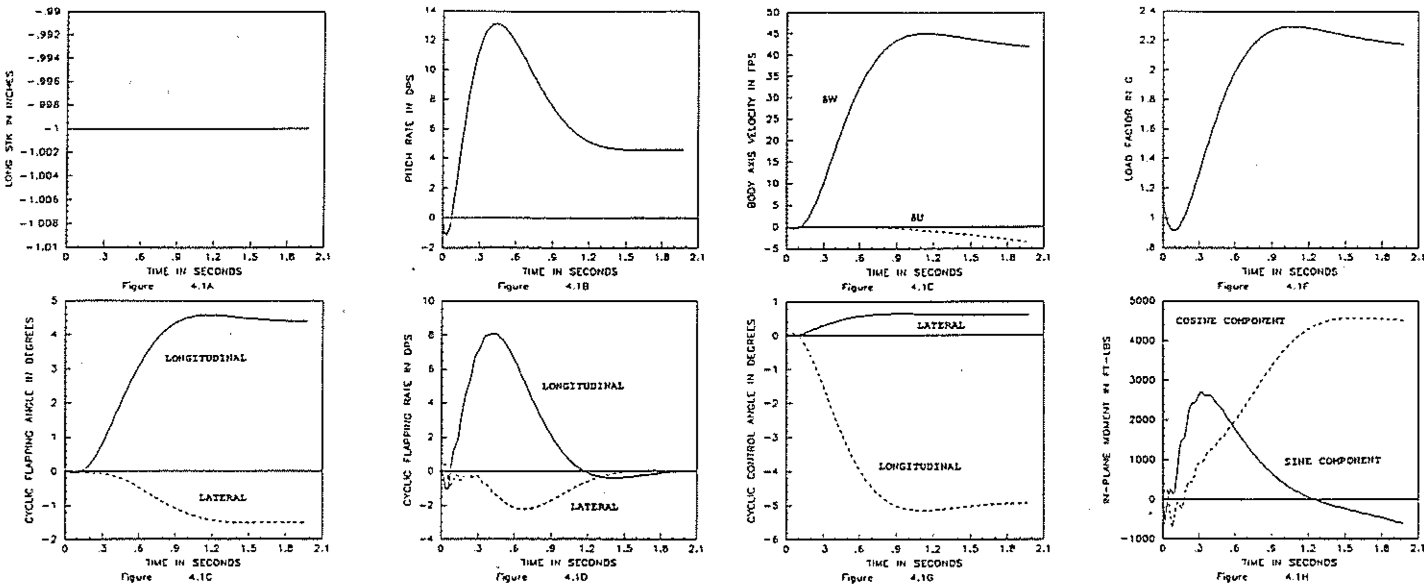

Figure 4-1: Closed-Loop Longitudinal Stick Step Responses
When Short Period Mode is Shaped to
Minimize In-Plane Loads

Figure 4-1, continued

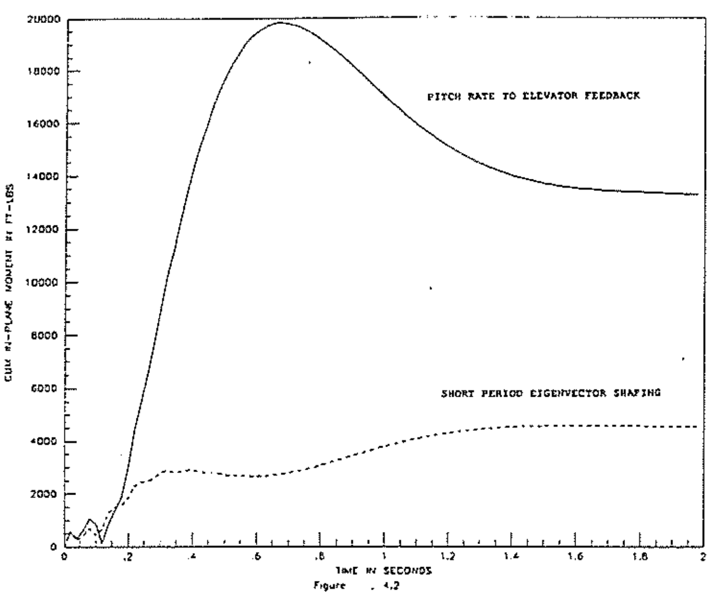

Figure 4-2: Comparison of Cumulative In-Plane Loads
Produced by Longitudinal Stick Step Input for
Pitch Rate to Elevator Feedback and Short Period
Mode Shaping Controllers

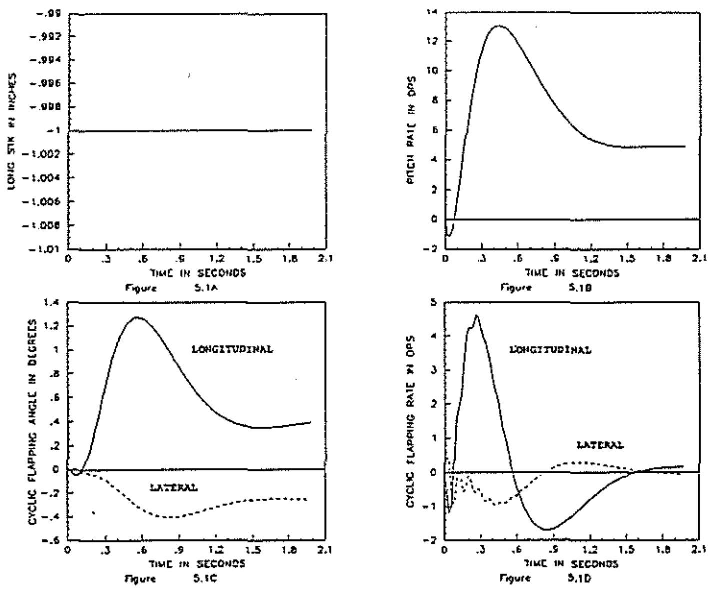

Figure 5-1: Closed-Loop Longitudinal Stick Step Responses for Reduced Authority In-Plane Loads Controller

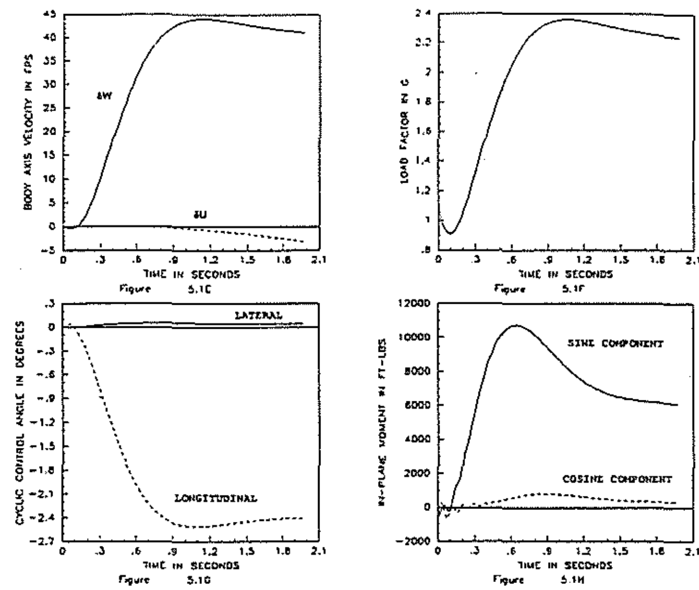

Figure 5-1, continued

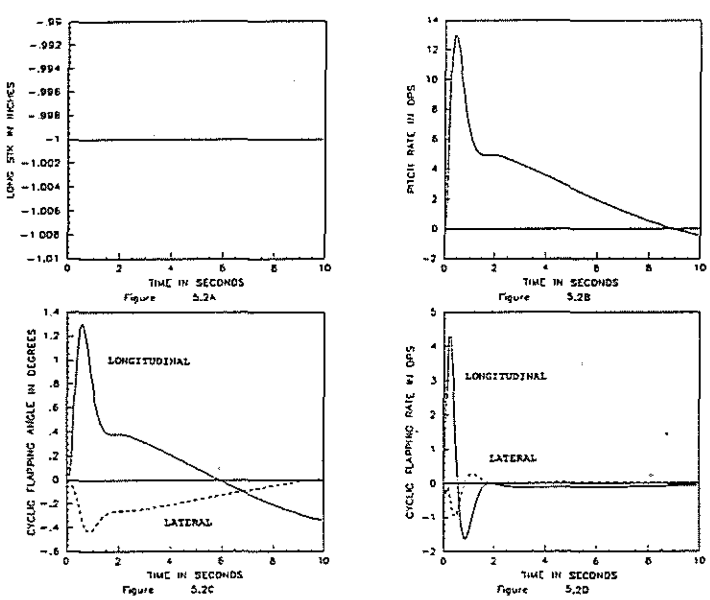

Figure 5-2: Closed-Loop Longitudinal Stick Step Responses For Finalized Combined Elevator and Rotor Cyclic Pitch Controller

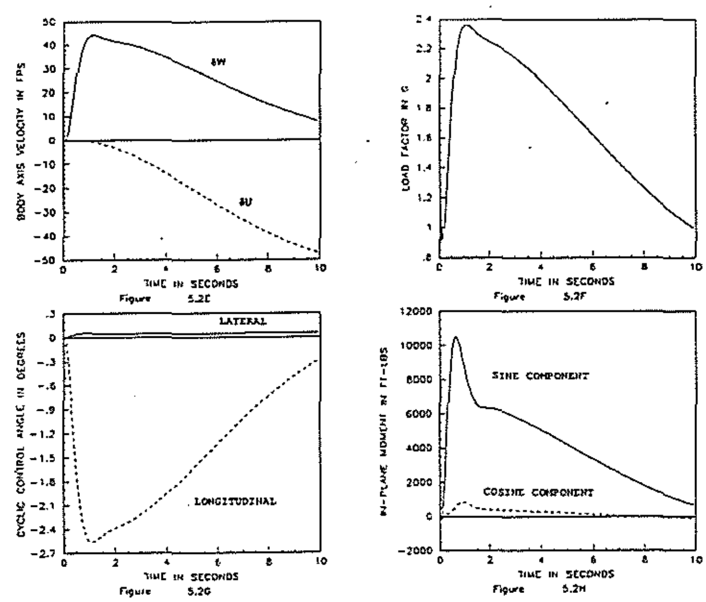

Figure 5-2, continued

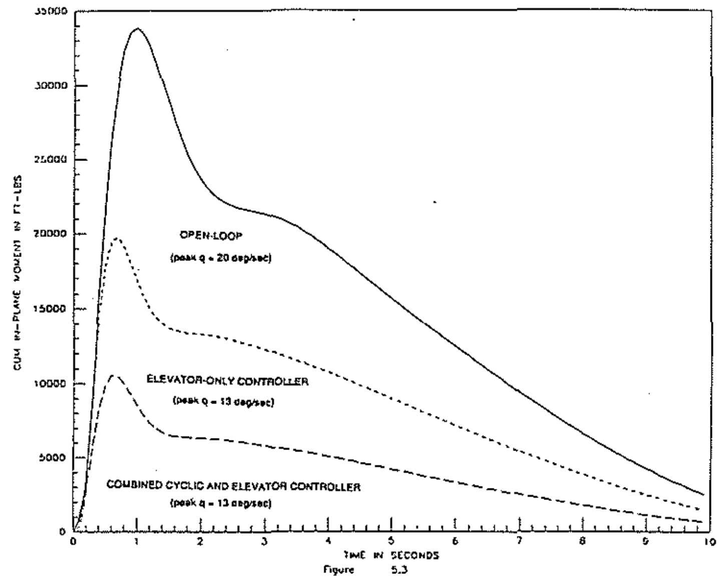

Figure 5-3: Comparison of Longitudinal Stick Step In-Plane Loads Responses for Various Controller Configurations

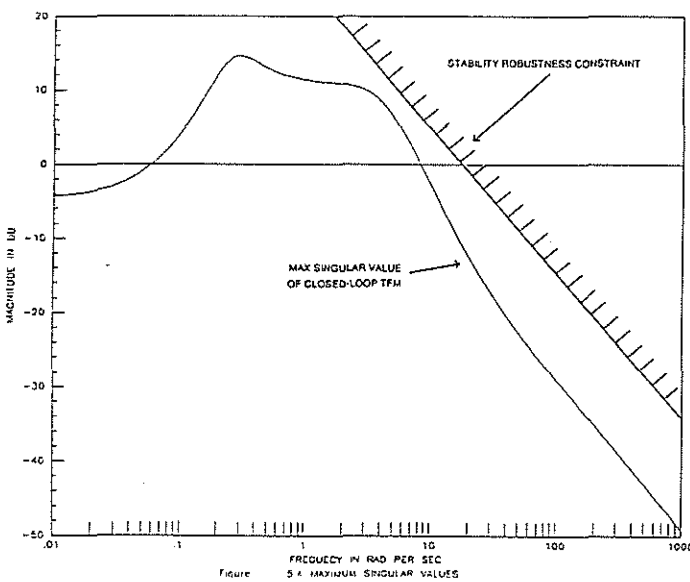

Figure 5-4: Stability Robustness Test for Finalized In-Plane Loads Controller

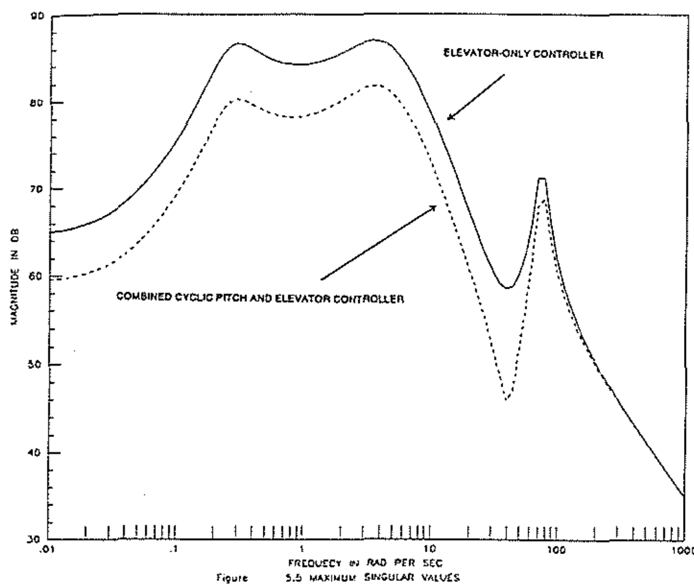

Figure 5-5: Bode Magnitude Plot of Output Sine Component of In-Plane Loads Produced by Longitudinal Stick Input